Asian Journal of Chemistry; Vol. 35, No. 3 (2023), 540-546

ASIAN JOURNAL OF CHEMISTRY

https://doi.org/10.14233/ajchem.2023.26890

Enhancement of Interfacial Wettability between Al-Zn Alloy Matrix and MnO_2 Decorated with Ni for Effective Cathodic Protection Systems

SUNIL JACOB[1,*], K.K. BINOJ[1], DONA BENNY[2] and P.Y. JINU[1]

[1]Department of Chemistry, Catholicate College Pathanamthita (Affiliated to Mahatma Gandhi University), Kottayam-689645, India
[2]Department of Physics, Madras Christian College, Chennai-600059, India

*Corresponding authors: E-mail: suniljacob07@gmail.com

Received: 12 October 2022; *Accepted*: 29 November 2022; *Published online*: 27 February 2023; AJC-21142

Substrates made of steel used in coastal applications are regularly exposed to harsh salty environments; as a result, it is essential to adopt reliable strategies for preventing corrosion. Utilization of aluminum rich sacrificial anodes is an efficient anticorrosive technique owing to its high columbic amplitude, low density, inherent negative potential and galvanic economy. In this work, the electrochemical and micro-structural was characterized by catalytic effect of MnO_2-Ni on anode activation. MnO_2-Ni present in anode matrix results in destroyed passive alumina film and facilitates the galvanic growth on an anode. The anode exhibited active operating potential and high columbic efficiency during prolonged marine exposure studies. High anodic efficacy was performed by fine tuning composites into the metal matrix Al based alloy. The results revealed that the preferential dissolution of intermetallic particles induced effective sacrificial anode action.

Keywords: Aluminium, Corrosion, Sacrificial anode, Weight loss, Cathodic protection.

INTRODUCTION

Corrosion occurs when metal reacts with its surroundings and deteriorates on its own. Numerous methods like changing aggressive nature of media, applying suitable corrosion inhibitors, using protective coatings and cathodic protection can be employed to mitigate corrosion [1-3]. Among these methods, anodic sacrificial action commonly accepted as the most efficient especially for offshore substrates and ships. Most of the process is progressed by the direct current impressed or the attachment of sacricial anodes such as magnesium, aluminum or zinc. Maximum studies conducted in the field was centered on Al rich Zn sacrificial anode where Zn destabilize the Al_2O_3 layer because of $ZnAl_2O_4$ spinel formation and the Zn concentration is optimized to 5 wt.% because of enhancement in metallurgical and electrochemical factors of alloy through β-phase formation [4]. Recent developments in this field were the solid ceramic particles incorporating into metal matrix. Discontinuously reinforced aluminum metal matrix composites exhibit blending properties of both composites and matrix results in substantial enhancement in physico-chemical and galvanic characteristics [5]. Incorporation of metal composites could also suppress and improve grain boundary metal corrosion.

It is well known that the production and functioning of metal matrix composites are influenced strongly with the interface between composite and the matrix and the wetting nature of composites with molten metal [6]. In the solidification process of metal matrix composites, the wettability of the reinforcement matrix by molten metal, which forms the matrix of a composite is especially crucial for creating a strong interface that allows effective distribution and transfer of loads from the matrix to the reinforcements [7]. Metallic coating on the composites is relatively inexpensive and have been successfully used to enhance wettability and to reduce interfacial reaction, moreover it also prevents the diffusion of liquid metal in to the composite [8]. The most important metals used to coat the composites are copper and nickel [9]. The incorporation of optimum amount of nickel in to manganese oxide remarkably enhances its capacitive performance, high power property, good cycling stability and moreover the presence of MnO_2 in aluminum matrix can form $MnAl_6$, which in turn significantly improves both psycho-chemical and metallurgical characteristics of aluminum metal matrix [10-13]. In these terms, this study explored the nickel deposited MnO_2 for making high performing Al-Zn alloy matrix sacrificial anodes with a view of its enhanced wettability.

EXPERIMENTAL

Experimental procedure for nickel deposition: Commercially available MnO_2 (Merck, India; ≥ 99.90%) with average grain size from 7 to 10 μm were ball-milled for 2 h initially for breaking the agglomerates. For the electroless deposition of nickel, a bath with specific composition containing 5 g L^{-1} tetrabutylammonium bromide (TBAB); 0.5 g L^{-1} sodium acetate; 15 g L^{-1} sodium citrate; 20 g L^{-1} sodium hypophosphite and 35 g L^{-1} nickel sulphate [14,15] was selected. During the nickel coating, this bath was stirred with a magnetic stirrer for 2 h at 80-85 ºC for reducing the settling of powder, while maintaing the pH at 6. For each coating, 10 g of MnO_2 powder was coated in 250 mL of electroless nickel solution.

Preferential wetting-sessile drop method: The sessile drop technique, which is based on the measurement of work of adhesion, was used to investigate the wetting properties. The experiments were carried out using Al-Zn alloy plate with 4 mm diameter and pure MnO_2; MnO_2-Ni (0.01, 0.1, 0.2, 0.5, 1.0, 2.0 wt.%) pellets. Before the experiment, Al-Zn alloy and the composites were cleaned ultrasonically; after this the MnO_2-Ni and MnO_2 substrate was horizontally placed in a chamber and the Al-Zn plate was placed in a dropping device. Chamber was evacuated in 5×10^{-4} Pa vacuum and heated at the desired 20 ºC min^{-1} heating rate. After the pressure and temperature stabilization, molten Al-Zn was removed slowly from the dropping device on a solid substrate by gradually decreasing the pressure to 0.11 MPa. The initial Al surface oxide, at the same time was removed mechanically as these liquid passes from the hole. When the solid substrate and molten Al-Zn comes in contact, a image was taken defining is as drop profile on zero time. The images were analyzed in ADSA program (Axis-Symmetric Drop Shape Analysis) for estimating the contact angle [16].

Anode casting process

Surface pretreatment: Commercially available zinc and aluminium rectangular blocks were employed as casting substrate. These were then polished using silicon carbide papers of 100, 250 and 600 grit in successions and with a paste of 0.5 μ alumina. These blocks were then cleaned as per ASTM G39 and then thoroughly washed using double distilled water and finally dried on 60 ºC.

Anode fabrication: Commercially available pure Zn (99.95%) and Al (99.90%) ingots were explored to fabricate Al + 5% Zn anodes. The metal ingots were cut, weighed and then melted in a muffle furnace at 710 ± 10 ºC using a graphite crucible. The number of MnO_2-Ni composites were introduced to the alloy with constant stirring and then homogenized with a SiC rod. The alloy melt with composite was once again keep for 15 min more in muffle furnace and finally introduced into a preheated graphite die of 5.5 cm × 3.5 cm × 0.5 cm dimensions.

Surface finishing: Polishing of the casted metal alloy matrix composite anodes was done using various grades of emery papers down to 600 and then de-greased with acetone and ethylene. After being polished, the anodes were rinsed in water and left to dry. The surface cavity was washed with a chromic acid and oxalic acid mixture for 5 min to eliminate any potential contaminants.

Characterization

Metallurgical characterization: The metallurgical characterizations of the anodes were carried out using Hitachi S-2400 scanning electron instrument. A small piece of the surface of the manufactured in large quantities sacrificial anode was taken as a representative sample. The anodes were etched with 1% NaO_2 solution by dipping for 45-60 sec, rinsed, washed, dried and finally characterized by secondary electron signal. The fabricated anodes were analyzed using an atomic force microscopy (Agilent-5500). Its values were estimated in contact mode with a Vista T-Cantilever with 0.2 N m^{-1} spring constant and 1 Hz frequency. Vickers microhardness indenter was used to evaluate the mechanical hardness in accordance with ASTM 384-89. Each anode samples were subjected to measure hardness values at five different positions of anode and the mean number were provided here.

Electrochemical characterization

Open circuit potential (OCP) decay: For two months, the open circuit potential has been tracked in real time, defined as the potential difference between the test anodes relative to the saturated calomel electrode (SCE) used as a reference. The potential-time variation was conducted to observe the rate of fluctuation of potential to know the active behaviour of anode. A copper wire was plugged into the anode after it was submerged in electrolyte. The electrode-electrolyte interface can be studied in terms fluctuations in OCP shift for total 60 days. All the samples were dipped in 3% NaCl solution at 30 ± 2 ºC. An oscillating temperature probe (OCT) was recorded after every minute for the first several days and then every 24 h for next 60 days.

Closed circuit potential (CCP) evaluation: When anode samples were galvanically linked to a large cathode with a surface area of 1:10, a closed circuit potential (CCP) was measured. The anode surface current density has been maintained constant by varying the regulating resistance.

Self corrosion rate: The casted anode samples were dipped in 3% NaCl solution for 90 days. The fixed region of anode was exposed, while the rest of the surface was insulated using teflon tape. The electrolyte was kept stagnant and the temperature was regulated to 30 ± 2 ºC. During the course of 90 days experimental period, the concentration of the electrolyte was depleted. To avoid this and maintain the electrolyte balance, new electrolytes are regularly introduced. After thoroughly cleaning the anodes in accordance with ASTM G 31, the reduction in the weight loss data had been analyzed by considering the pre- and post-immersion weight of the samples. From this weight loss, the rate of self-corrosion has been calculated using the following eqn.:

$$\text{Rate of self corrosion} = \frac{\text{Anode weight loss}}{\text{Surface area of the anode} \times \text{Time period}}$$

Potentio-dynamic cyclic polarization: Linear sweep voltammetry (LSV) was carried out using an Autolab 80 plus FRA2 corrosion system. The electrolyte used was aqueous

3% NaCl solution. The Ag/AgCl, Pt and the anodes having 1 cm^2 exposed area were used as reference, counter and working electrodes, respectively. The polarization experiments were repeated to test reproducibility. The anodes were equilibrated in 3% NaCl solution for sufficient time prior to each polarization at a scan rate of 0.005 V s^{-1}.

Electrochemical impedance analysis: An electrochemical analyzer, Auto lab PG stat 30 plus FRA 2 was used to analyze the impedance characteristics. The electrolyte used was 3% NaCl. The Ag/AgCl, Pt and the anode having 1 cm^2 exposed area were used as reference, counter and working electrodes, respectively. The frequency scanned from 1 MHz to 0.1 Hz with reference to OCP after 60 min exposure of the sample in the electrolyte.

RESULTS AND DISCUSSION

Interfacial wettability: Anodes made up of metal should be activated by wetting the molten Al-Zn alloy using composite. Effective wetting can be described in terms of contact angle (θ) and surface tension of liquid [6]. The magnitude of contact angle describes the wettability as θ = 0º for perfect wetting; θ = 180º no wetting and 0º < θ < 180º for partial wettability. A low contact angle is an indication of the high wettability of material. A correlation between the wt.% of MnO_2, MnO_2-Ni composite and the contact angle in molten Al-Zn alloy is shown in Fig. 1. The Al-Zn anode showed a significant decrease in the contact angle with MnO_2-Ni when compared to pure MnO_2. This demonstrated that the composite was successfully modified with a nickel-coated interface, leading to a decrease in the solid/liquid interfacial energy [17]. Due to an increase in surface energy, contact angle didn't change significantly at low concentrations of composite (0.01 wt.%) [6].

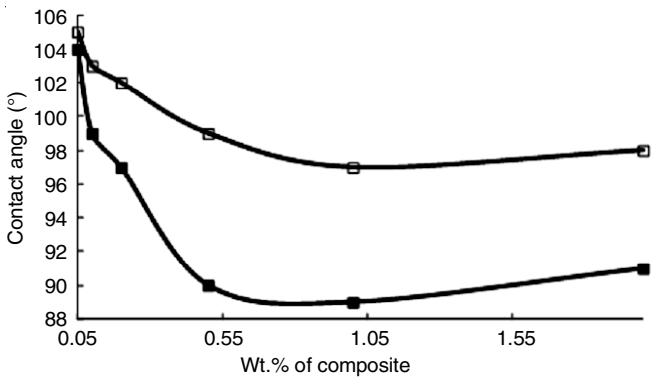

Fig. 1. Correlation of wt.% of the composite (□) MnO_2, (■) MnO_2-Ni with contact angle

Anodes made of pure Al-Zn have a contact angle of 106º, but adding even a small amount of MnO_2-Ni can bring the angle down to 99º. Table-1 shows that a 1 wt.% increase in MnO_2-Ni results in a further reduction to 94º. Fig. 2 displays the wetta-bility percentage of nickel-coated MnO_2 composite and pure MnO_2 with molten aluminium alloy. Wetting improves with increasing composite weight (wt.%), which indicate that the wettability mechanism works even at the low concentrations of composite; thus, nickel-coated MnO_2 composite displays a significant higher wettability than uncoated MnO_2 composite, which is attributed due to the solubilization of coated metallic nickel in the aluminium alloy matrix.

TABLE-1
CONTACT ANGLES BETWEEN Al-Zn ALLOY WITH MnO_2 (θ_1) AND MnO_2-Ni (θ_2)

Amount of composite (wt.%)	Contact angle (θ_1)	Contact angle (θ_2)
0.05	105	104
0.10	103	99
0.20	102	97
0.50	98	90
1.00	97	89
2.00	98	91

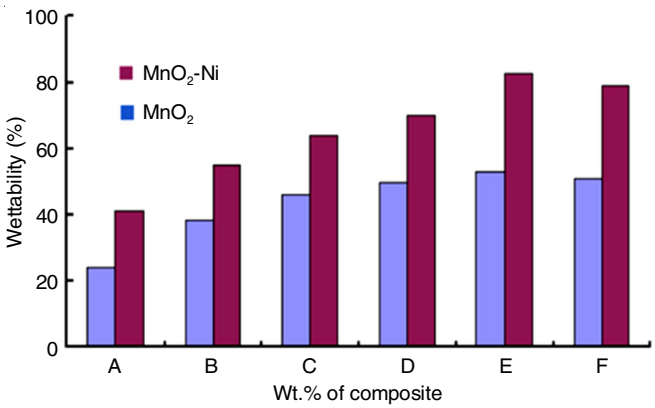

Fig. 2. Comparison of the extent of wettability of Al-Zn-In anode with different wt.% of MnO_2 and MnO_2-Ni respectively (A) 0.05%; (B) 0.1%; (C) 0.2%; (D) 0.5%; (E) 1%; (F) 2%

Several other important parameters such as surface finish of the solid, purity of the melt, composition, temperature and pressure have also significant influence on the contact angle (θ) measurement. Furthermore, it was sometimes hard to control these characteristics, and the literature is riddled with conflicts and inaccuracies because of measurement errors.

Morphological and microstructural studies: Fig. 3a-b demonstrated the morphology of MnO_2 incorporated Al-Zn and MnO_2-Ni with Al-Zn anode. The aluminium anode, like the composite included alloy anodes, was cast with a spangles-like finish. Intermetallic particles were appeared to be bright in image because of higher atomic number in comparison with the Al matrix as shown in Fig. 3. The large particles called the constituent particles were observed in both MnO_2-Ni and MnO_2 incorporated anodes. A large number of fine particles (50-200 nm white dots of < 0.5 μm) also known as dispersoids were present in nano-MnO_2 incorporated anode and similar to that of MnO_2-Ni incorporated one. However, the size of the intermetallic particles is larger in MnO_2 incorporated Al-Zn anode and also their distribution is not uniform as compared to MnO_2-Ni incorporated anode. Generally, presence of the large micrometer sized intermetallics particles causes localized dissolution, initiating on the particle-matrix boundary regions and resulted in higher non-columbic metal loss of anode [18]. Hence, the presence of smaller intermetallic particles and their uniform distribution can have significant effect on the galvanic and metallurgical performances of the anode.

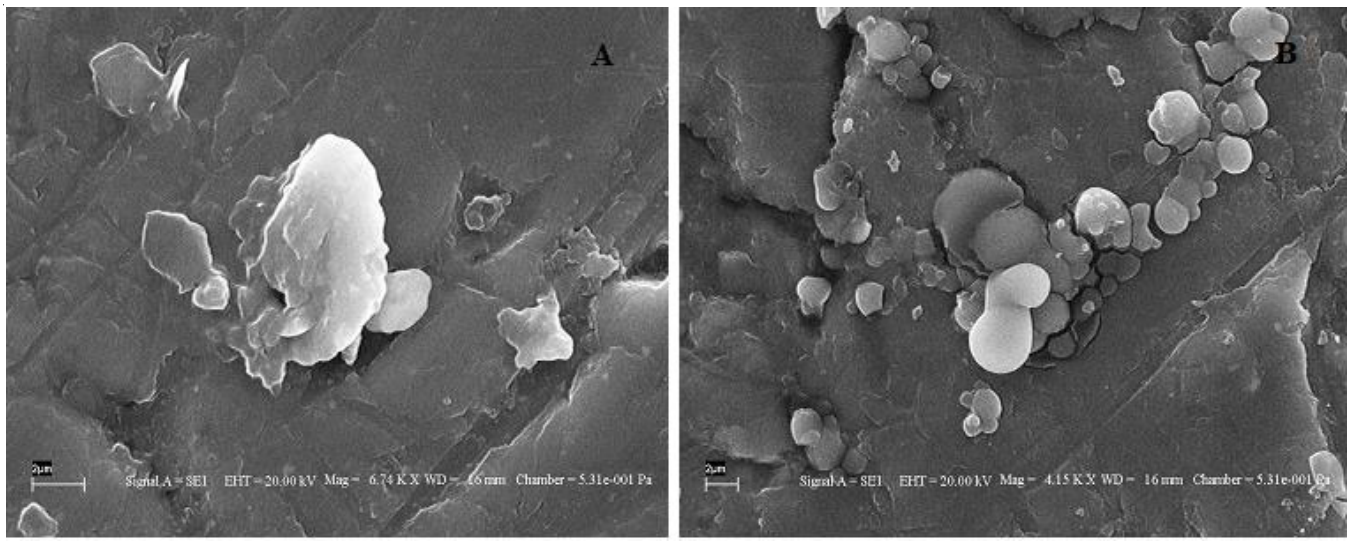

Fig. 3. SEM micrographs of Al-Zn incorporated with nano MnO_2 (a), MnO_2-Ni (b)

Fig. 4a-b depict the concurrent AFM topography of MnO_2 incorporated Al-Zn anode whereas Fig. 4c-d show the AFM topography MnO_2-Ni with Al-Zn anode. During the investigation, a significant difference in the topography between two anodes became noticeable. Generally, both anodes exhibited the constituent particles (> 0.5 µm). However, MnO_2-Ni incorporated anode have well defined smaller dispersoid in the matrix compared to MnO_2 incorporated anode. This result was in well accordance with the morphological characterization by SEM images. Thus, it was established that MnO_2-Ni incorporation results in the formation of fine intermetallics of uniform size, which is a desirable condition for efficient metallurgical enhancement of the anode.

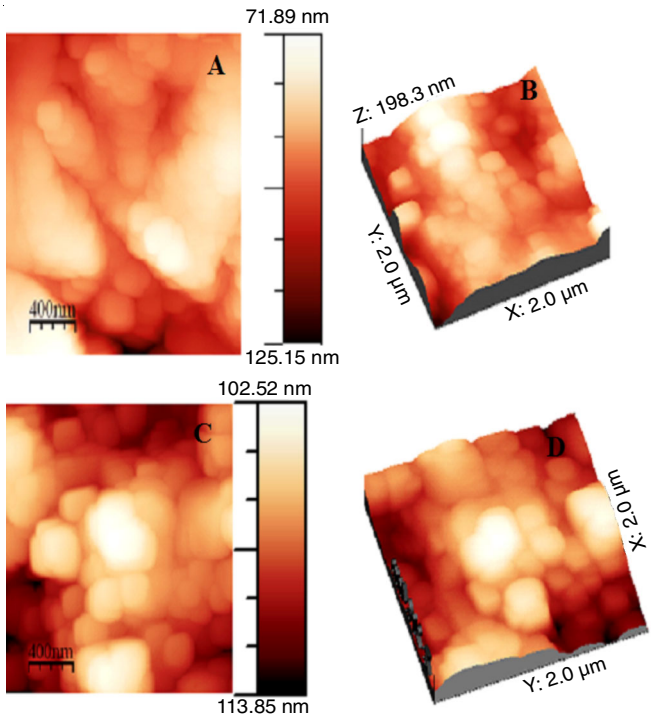

Fig. 4. AFM micrographs of Al-Zn + MnO_2 (a), Al-Zn + MnO_2-Ni (c); (b) and (d) are 3-D view

Open circuit potential (OCP) decay studies: After 2 months of immersion, the OCP values of MnO_2-Ni containing anodes changed from the -0.960 to -0.989 V range to -0.947 to -0.981 V range (Fig. 5). However, 0.5% MnO_2-Ni incorporated anode exhibits high OCP shift of -0.042 V in negative direction as compared to pure Al-Zn anode. This significantly large cathodic shift in OCP persisted for at least two months. Potential causes include cracking in sacrificial anodes and other forms of uneven corrosion of the anode [19].

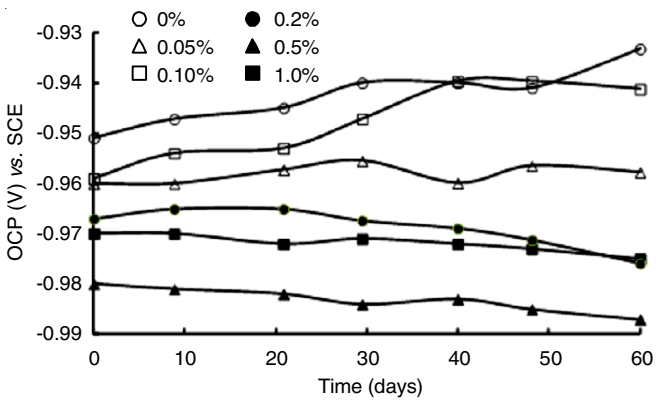

Fig. 5. OCP decay of Al-Zn anode incorporated with different MnO_2Ni

However, a significant anodic OCP shift was observed after an alumina passive coating was developed for the anode surface and the purity of Al-Zn anode was elevated [20]. Furthermore, the anodic dissolution reaction of Al-Zn anode is suppressed due to the enrichment of the hydrodynamic alumina layer on the anode surface, which reduces the rate of diffusion of dissolved oxygen on cathode. All the composite-integrated anodes outperformed pure Al-Zn anodes in terms of OCP value, but this was insufficient evidence for choosing the optimal anode. In this context, an in-depth analysis of anode performance was also conducted.

Closed circuit potential (CCP) evaluation: When the anode consumed during cathodic protection of the linked steel, the resulting potential is known as the closed-circuit potential

(CCP). The discrepancy between the CCP readings and real galvanic exposure is negligible since only a less amount of current flows through the electrode pair. Typically, CCP values are only recorded during the active galvanic responses. Because of this, the general pattern of change in CCP values may be taken into account as meaningful while assessing the anodic features.

The cathodic CCP values of the MnO_2-Ni-containing anode were much greater than those of bare Al anode, ranging from -0.928 to -0.979 V (Fig. 6). With respect to OCP values, the anodes that had 0.5% MnO_2-Ni showed the liveliest activity. Effective sacrificial anodes often have both active CCP and OCP, since a relatively noble potential denotes passivation. When the relatively stable oxide layer on the anode was broken down by a shift in CCP, thus the potential of anode dramatically swung to the cathode. Cathodic current is believed to boost the rates of hydrogen evolution sharply and active metal dissolution at a specific negative potential.

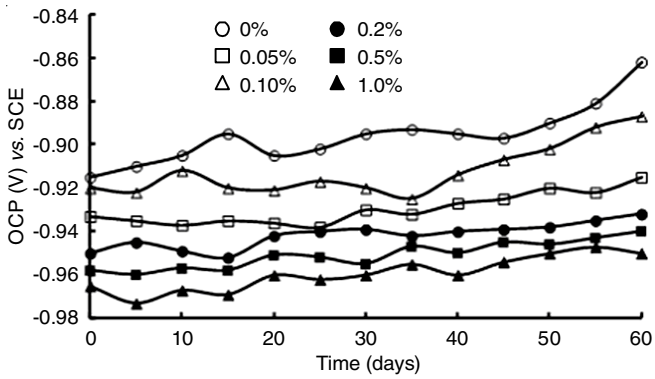

Fig. 6. Variation in CCP of the Al-Zn-In anodes with different amounts of MnO_2-Ni incorporation

Self corrosion rate: Estimation of self-corrosion values were obtained for Al-Zn sacrificial anodes, whose primary drawback was the loss of non-columbic metals. Fig. 7 depicts the self-corrosion values of anodes for two months of exposure in 3% NaCl. All anodes incorporate with composited show the self-corrosion values in 13.880 to 6.994 μg cm^{-2} h^{-1} range whereas bare Al-Zn anode exhibits the low self-corrosion. According to the OCP decay and polarization investigations, 0.5% composite integrated anode had the lowest self-corrosion values. Reduction in the values of self-corrosion for an anode was due to the reduction of grain-boundary corrosion owing to better refinement of grains [21]. A suitable metallic coating on composite can act as wetting agent as well as *in situ* hybridizing agent [7], which provides enhanced mechanical strength to the matrix. An intermetallic phase, if formed between in the coating and matrix, would strengthen the Al-Zn matrix, which effectively suppresses the non-columbic metal loss. A second hybridization reinforcement can be formed when dissolved nickel coating in Al-Zn matrix reacts with nickel coating on the MnO_2 composite material. By incorporating a second reinforcement directly into the matrix, a process known as *in situ* hybridization, the self-corrosion rate of Al-Zn anode can be significantly decreased. Low self-corrosion rate is a need for an effective sacrificial anode for preventing frequent anode material replacement.

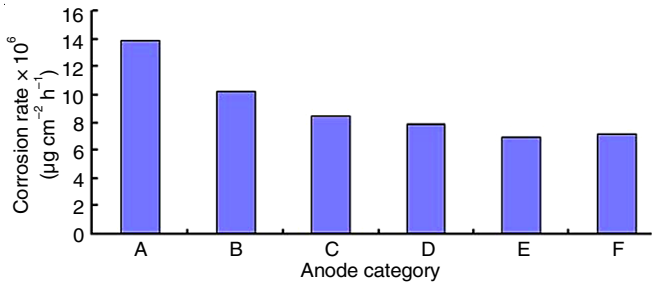

Fig. 7. Comparison self-corrosion rates of the MnO_2-Ni with Al-Zn: (A) 0%, (B) 0.05%, (C) 0.1%, (D) 0.2%, (E) 0.5% (F) 1%

Potentio-dynamic polarization: For MnO_2 and MnO_2-Ni incorporated Al-Zn alloy sacrificial anodes, the potentiodynamic polarization curves are shown in Fig. 8. Corrosion potential shifts to lower values when MnO_2-Ni was added to the Al-Zn anode as compared to when MnO_2 was added, [E_{corr} (corrosion potential) shifted from -0.968 to -0.894 V *vs.* Ag/AgCl], a desirable factor for an effective system of cathodic protection. The anode with MnO_2 showed a lower E_{corr} value and a wider passive zone in the polarization curve. The metal surface has formed oxide layers to prevent further corrosion. I_{corr} of the anodes varied from 3.141 to 3.106 A cm^{-2}. An increasing I_{corr} value is the indication of a sacrificial active/action character in the Al-Zn anode. Since the current density at the MnO_2-Ni integrated Al-Zn anode was higher than that of MnO_2 integrated Al-Zn anode, indicated that the Al-Zn anode was significantly more active than MnO_2 integrated Al-Zn anode. It was hypothesized that during anode production, corrosion would be enhanced if the intermetallic phases formed and acted as additional cathodic sites.

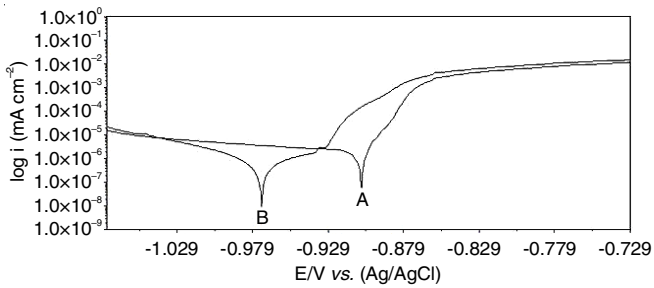

Fig. 8. Potentiodynamic polarization behaviour of Al-Zn anode incorporated with MnO_2 (A) and MnO_2-Ni (B) in 3% NaCl solution

Electrochemical impedance characterization: Fig. 9 displays EIS data of bare anode and MnO_2-Ni incorporated anode. Pure anode exhibit a large arc in the high frequency region as evidenced by impedance plots. A similar arc was also observed for the MnO_2-Ni incorporated anode. This indicates that the anodes follow homogeneous galvanic reaction paths [22]. On the other hand, it was discovered that the polarization resistance (R_p) values of the anode having MnO_2-Ni integrated were lower than bare anode. The lowering of surface resistivity was prerequisite for an efficient cathodic protection system [23]. It is possible that the dominant and broad arc observed in the Nyquist plots of MnO_2-Ni anodes can be attributed to the generation of a thin alumina layer on their outermost surface. In addition, when the anode performs an efficient sacrificial

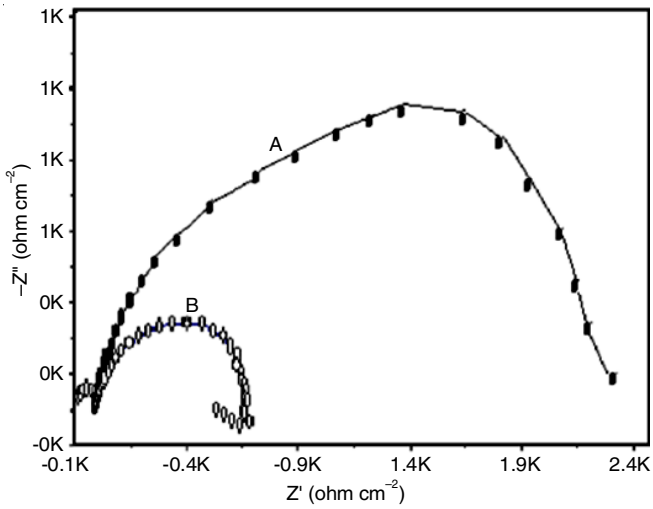

Fig. 9. Nyquist diqgram of the Al-Zn-In anodes in 3% NaCl solution in the requency range of 1 MHz with reference to (A) bare Al-Zn-In anode, (B) MnO_2-Ni incorporated anode

action, an intermediate state may be attributed to its appearance as a result of an inductive loop in the low frequency area [24].

Incorporating MnO_2-Ni into the Al alloy anode results in a noticeable shift in the Z modulus (Fig. 10). In comparison to a blank anode, the Z modulus of an Al alloy anode having MnO_2-Ni matrix showed a lower value and the linear slope modulus fell progressively [25]. Theoretically, at lower frequencies, when the Z modulus is smaller, the sacrificial action of the anode is thought to be most effective. The phase angle plotted against logarithm of the frequency is shown in Fig. 10. Blank anode impedance spectra showed a phase angle of about 70º across very narrow frequency ranges, whereas MnO_2-Ni containing anode spectra showed a phase angle of just 50º. The successful instability of the passive alumina coating on the anode surface was ascribed to the reduced phase angle values of MnO_2-Ni anodes. It was widely known that pure capacitive character plotted as the phase angles gradually increase and reaches to 90º. A reduction in the phase angle and R_p values is a clear implication of enhanced sacrificial dissolution of anode [26].

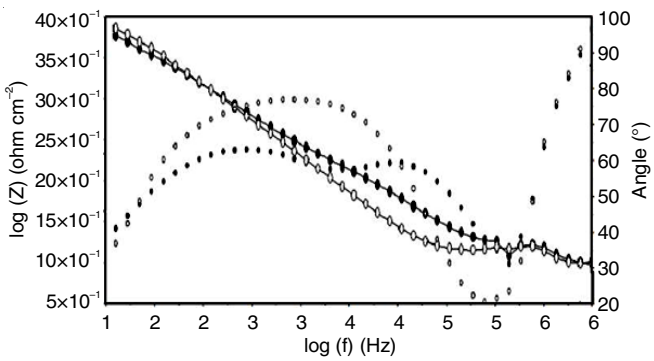

Fig. 10. Bode and phase angle "plots of the Al-Zn-In anode with MnO_2-Ni incorporation (o) bare Al-Zn-In anode, %, (•) MnO_2-Ni incorporated anode

Comparative evaluation: The physico-chemical and galvanic characteristics of the reported MnO_2 incorporated Al-Zn anodes [11] and the same results from the present study was also compared. Matrix alloying modifies the composition of the matrix material and the nickel coating on the composite improves the wettability of the reinforcement. This led to the enhancement in the deformation resistance of anode and hence the hardness was changes from 52 ± 1.4 (Al-Zn + MnO_2) to 83 ± 2.7 (Al-Zn + MnO_2-Ni) VHN. Moreover, the coating of nickel reduced the micropores at its interface and enhances the bonding strength; however, composite can more effectively with stand local deformation. The CCP and OCP decay trend of MnO_2-Ni incorporated anode exhibited more active behaviour than MnO_2 incorporated anode. The OCP values of anodes incorporated with MnO_2 incorporated anode exhibited OCP -0.960 to -0.989 V, indicating the active nature of MnO_2-Ni incorporated anode. The self-corrosion rate of MnO_2 incorporated was 7.861 µg cm^{-2} h^{-1} and that of MnO_2-Ni incorporated anode exhibited only 6.994 µg cm^{-2} h^{-1} in 3% NaCl, as a result of *in situ* alloying of nickel coating with metal matrix. Due to the successful suppression of secondary cathodic reactions at the interface as the metallic coatings on the modified surface interfaces, the galvanic efficiency, a fundamental factor to measure the value of a sacrificial anode in a marine environment, increased dramatically from 80% to 89.2%. In addition, the MnO_2-Ni anode can resist extreme polarization during the normal anode operation too.

Conclusion

The incorporation of MnO_2-Ni composite in to Al-Zn alloy anode yielded high metallurgical and galvanic characteristics due to enhanced wettability. The physico-chemical and electrochemical results revealed that the nickel coating acted as a wetting agent but also *in situ* alloying element. An incorporated anode with 0.5% optimum quantity MnO_2-Ni showed highly active OCP due to formation of the thin passive oxide layer on the surface of anode; which also resist the severe polarization during the galvanic exposure studies. The optimum concentration of MnO_2-Ni on the Al-Zn alloy is significant for the effective activation of anode as other combinations had adverse or negligible effect. A high galvanic efficiency of 89.2% was achieved during long-term evaluation owing to the effective suppression of the non-columbic metal loss. According to the electrochemical impedance spectra, the addition of MnO_2-Ni on the Al-Zn alloy significantly reduced the polarization resistance value, a necessary condition for the cathodic protection systems that work well.

CONFLICT OF INTEREST

The authors declare that there is no conflict of interests regarding the publication of this article.

REFERENCES

1. A.E.-A.S. Fouda, S.A. Abd El-Maksoud, E.H. El-Sayed, H.A. Elbaz and A.S. Abousalem, *RSC Adv.*, **11**, 13497 (2021); https://doi.org/10.1039/D1RA01405F
2. E. Ghiamati Yazdi, Z.S. Ghahfarokhi and M. Bagherzadeh, *New J. Chem.*, **41**, 12470 (2017); https://doi.org/10.1039/C7NJ01655G

3. C.J. Li and M. Du, *RSC Adv.*, **7**, 28819 (2017); https://doi.org/10.1039/C7RA03709K
4. S.M.A. Shibli and V.S. Gireesh, *Corros. Sci.*, **47**, 2091 (2005); https://doi.org/10.1016/j.corsci.2004.09.010
5. Y. Zhan and G. Zhang, *Mater. Lett.*, **57**, 4583 (2003); https://doi.org/10.1016/S0167-577X(03)00365-3
6. J. Hashim, L. Looney and M.S.J. Hashmi, *J. Mater. Process. Technol.*, **119**, 329 (2001); https://doi.org/10.1016/S0924-0136(01)00919-0
7. T.P.D. Rajan, R.M. Pillai and B.C. Pai, *J. Mater. Sci.*, **33**, 3491 (1998); https://doi.org/10.1023/A:1004674822751
8. C.A. Leon and R.A.L. Drew, *J. Mater. Sci.*, **35**, 4763 (2000); https://doi.org/10.1023/A:1004860326071
9. S. Abraham, B.C. Pai, K.G. Satyanarayana and V.K. Vaidyan, *J. Mater. Sci.*, **27**, 3479 (1992); https://doi.org/10.1007/BF01151823
10. A.A. Hamid, P.K. Ghosh, J.C. Jain and S. Ray, *Wear*, **260**, 368 (2006); https://doi.org/10.1016/j.wear.2005.02.120
11. S.M.A. Shibli and K.K. Binoj, *J. Appl. Electrochem.*, **39**, 159 (2009); https://doi.org/10.1007/s10800-008-9659-3
12. P.C. Maity, P.N. Chakraborty and S.C. Panigrahi, *Mater. Lett.*, **20**, 93 (1994); https://doi.org/10.1016/0167-577X(94)90068-X
13. A.A. Hamid, S.C. Jain, P.K. Ghosh and S. Ray, *Metall. Mater. Trans., A Phys. Metall. Mater. Sci.*, **36**, 2211 (2005); https://doi.org/10.1007/s11661-005-0340-8
14. S. Zhang, Q. Li, X. Yang, X. Zhong, Y. Dai and F. Luo, *Mater. Charact.*, **61**, 269 (2010); https://doi.org/10.1016/j.matchar.2009.10.006
15. I.H. Oh, J.Y. Lee, J.K. Han, H.J. Lee and B.J. Lee, *Surf. Coat. Technol.*, **192**, 39 (2005); https://doi.org/10.1016/j.surfcoat.2004.04.064
16. E. Rocha-Rangel, P.F. Becher and E. Lara-Curzio, *Interface Anal.*, **35**, 151 (2003); https://doi.org/10.1002/sia.1525
17. C.A. Leon and R.A.L. Drew, *J. Mater. Sci.*, **35**, 4763 (2000); https://doi.org/10.1023/A:1004860326071
18. A. Davoodi, J. Pan, C. Leygraf and S. Norgren, *Electrochim. Acta*, **52**, 7697 (2007); https://doi.org/10.1016/j.electacta.2006.12.073
19. S.Z.E. Abedin and F. Endres, *J. Appl. Electrochem.*, **34**, 1071 (2004); https://doi.org/10.1023/B:JACH.0000042672.23588.df
20. H. Sina, M. Emamy, M. Saremi, A. Keyvani, M. Mahta and J. Campbell, *Mater. Sci. Eng. A*, **431**, 263 (2006); https://doi.org/10.1016/j.msea.2006.06.011
21. S.M.A. Shibli, S.R. Archana and P. Muhamed Ashraf, *Corros. Sci.*, **50**, 2232 (2008); https://doi.org/10.1016/j.corsci.2008.06.017
22. G.L. Song, *Corros. Sci.*, **51**, 2063 (2009); https://doi.org/10.1016/j.corsci.2009.05.031
23. S.M.A. Shibli and S. George, *Appl. Surf. Sci.*, **253**, 7510 (2007); https://doi.org/10.1016/j.apsusc.2007.03.052
24. J. He, J. Wen and X. Li, *Corros. Sci.*, **53**, 1948 (2011); https://doi.org/10.1016/j.corsci.2011.02.016
25. A. Venugopal and V.S. Raja, *Corros. Sci.*, **39**, 2053 (1997); https://doi.org/10.1016/S0010-938X(97)00082-6
26. J.B. Bessone, D.R. Salinas, C.E. Mayer, M. Ebert and W.J. Lorenz, *Electrochim. Acta*, **37**, 2283 (1992); https://doi.org/10.1016/0013-4686(92)85124-4